Supplemental Document

Optics EXPRESS

Single-frame far-field diffractive imaging with randomized illumination: supplement

ABRAHAM L. LEVITAN,[1,*] KAHRAMAN KESKINBORA,[1,2,3] UMUT T. SANLI,[2] MARKUS WEIGAND,[4] AND RICCARDO COMIN[1]

[1]*Massachusetts Institute of Technology, 77 Mass Avenue, Cambridge, MA 02139, USA*
[2]*Max Planck Institute for Intelligent Systems, Heisenbergstrasse 3, 70569 Stuttgart, Germany*
[3]*Harvard University, John A. Paulson School of Applied Sciences, Center for Integrated Quantum Materials, 19 Oxford Street, Cambridge, MA 02138, USA*
[4]*Helmholtz-Zentrum Berlin für Materialien und Energie GmbH, 12489 Berlin, Germany*
[*]*alevitan@mit.edu*

Supplement DOI: https://doi.org/10.6084/m9.figshare.13154393

Parent Article DOI: https://doi.org/10.1364/OE.397421

Single-frame far-field diffractive imaging with randomized illumination: supplementary material

In this supplement, we provide additional information that may be helpful for researchers seeking to reproduce the results of the aforementioned paper. This includes the full set of parameters used in our numerical experiments, an expanded explanation of our zone plate design process, a discussion of the method used to calculate the Fourier ring correlation curves reported in the main paper, and a description of our fabrication method for the x-ray zone plate optics. In addition, we discuss our calculation of the resolution limit for reconstructions, further discuss the effect of the illumination intensity's nonuniformity, and provide a set of design considerations for RIP setups.

1. NUMERICAL EXPERIMENT PARAMETERS

We describe here the setup of our numerical experiments. Those interested in further inspecting the details of the experiments are encouraged to contact the authors for the original code.

In all cases, ideal BLR illumination was defined on an array with size larger than $2k_p \times 2k_p$, where k_p is the intended maximum probe frequency measured in pixels. To generate the illumination, a central circular region with a diameter $\frac{4}{5}$ of the array size is filled with uniform amplitude phase noise. This is then propagated into the far-field via a 2D Fourier transform. The region in Fourier space within $|k| = \frac{k_p}{2}$ is set to zero, as is the region outside $|k| = k_p$, leaving a ring in reciprocal space. This is then propagated back into the near field to form an ideal BLR probe for simulation.

Before simulating diffraction from the objects, the probes were upsampled by padding in Fourier space such that they are defined on an array of at least $(2k_p + 2k_o) \times (2k_p + 2k_o)$ pixels. This ensures that the multiplicative interaction between the probe and object doesn't lead to aliasing. We show the results of a typical ensemble of reconstructions from a randomly generated object in S1.

For the numerical experiments which discuss the impact of noise sources, all reconstructions were performed on a probe with maximum frequency $k_p = 128$ and a band-limiting frequency of $R = 0.4$. In each case, we performed reconstructions on between 50 and 200 randomly generated images per noise level. The error is determined from a square central region of the reconstructions, with a side length half that of the overall array, as shown in Figure S1d.

2. DESIGN OF RANDOMIZED ZONE PLATES

Our technique relies on illuminating a large region with highly speckled light containing high frequency components. This illumination function was achieved with diffractive optics that fill a clearly defined field of view with light whose intensity is as uniform as possible. The field of view is chosen to have a sharp drop-off simply so that the eventual reconstructions achieve comparable noise levels across the entire field of view. Other approaches which, for example, lead to a Gaussian envelope on the probe are equally applicable in principle, but lead to a less uniform noise profile in the reconstruction.

To generate these diffractive optics, we start by simulating a discretized light field that consists of uniform amplitude pure phase noise within a circular aperture whose diameter matches the intended final field of view diameter. We then numerically propagate this light field to the plane of our diffractive optic, and record the phase of the light field at each pixel. We generate a binarized optic with a specified outer diameter and beamstop diameter from this phase field. The zones are defined by setting all pixels with phase below a certain threshold to 0 and all other pixels to 1. This process matches the simplest "ZP_0" approach described in detail in [1]. This design process is further outlined visually in Supplementary figure S2. All zone plates used in this paper used a beamstop with a diameter of half the outer zone plate diameter.

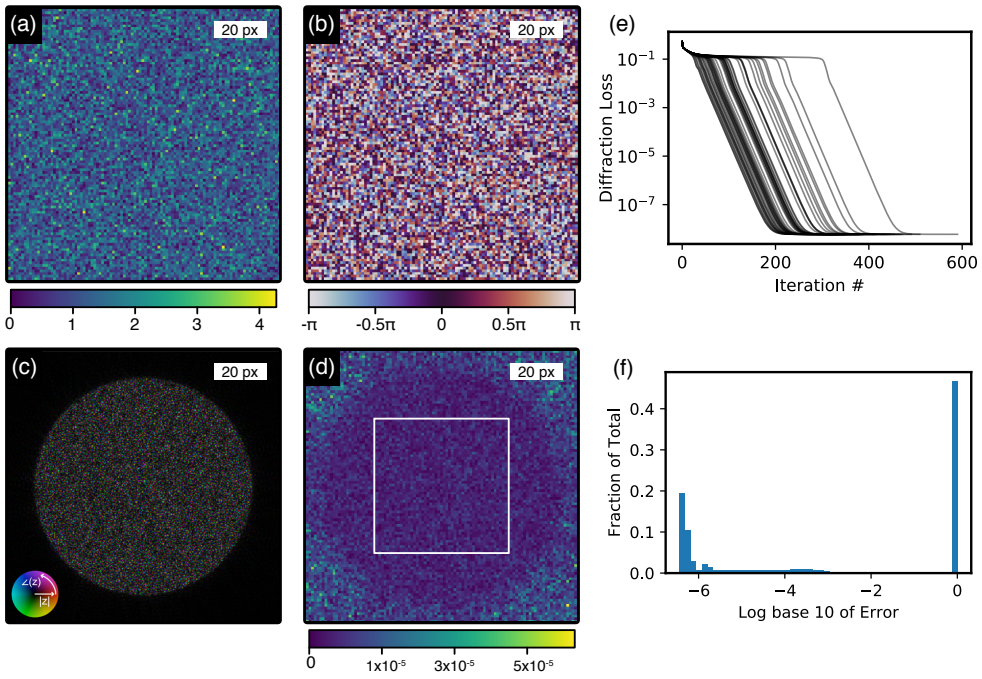

Fig. S1. Typical Reconstruction. (a), (b) the amplitude and phase of a typical random object. (c), a typical randomized probe used in the simulations. (d), The magnitude of the difference between a completed noise-free RPI reconstruction and the ground truth, with the central region from which error is reported marked in white. (e) The progression of diffraction loss over time for 50 independently initialized reconstructions on the same typical diffraction pattern. (f) The distribution of final RMS error for all reconstructions reported in Figure 3a.

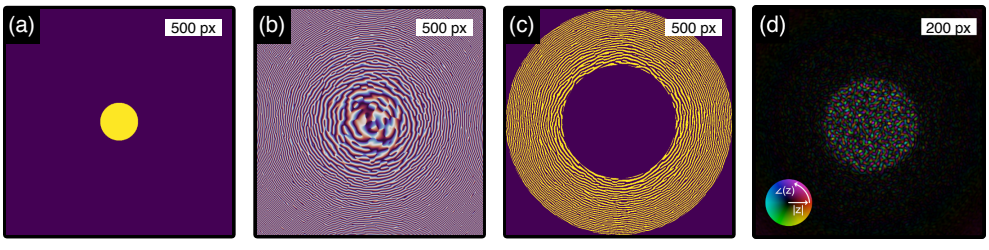

Fig. S2. Optics Design. (a), The amplitude of the initial focal spot, filled with randomly varying phase. (b), The phase of this focal spot, propagated to the plane of the optic. (c), The binarized optic defined from this phase distribution. (d), The focal spot simulated from this binarized optic.

3. EXPERIMENTAL RESOLUTION CALCULATIONS

All reported resolutions were calculated via the Fourier Ring Correlation (FRC)[2] method, by comparison with ptychography results captured from the same sample region. Although this is potentially an underestimate of the true resolution if (as we saw in our reconstructions from FeGd samples) the ptychography itself exhibits pathologies, we believe that it is a conservative estimate which addresses the fundamental question of how RPI compares with ptychography.

In each case, we started by cutting out a region of the ptychography scan which overlapped with a region of the RPI reconstruction entirely within the RPI field of view. This ptychography cutout was then downsampled by extracting the central region in Fourier space corresponding to the band-limiting constraint in the RPI reconstruction. Any linear phase ramps in the RPI reconstructions (arising when the detector alignment shifts slightly between the calibration and RPI reconstructions) were manually removed and the cropped images were apodized with a Hann window. We then calculated a subpixel shift between the RPI and downsampled ptychography reconstructions and shifted the ptychography reconstruction to overlap with the RPI result. Finally, an FRC was calculated between the two images, excluding the outer 4 pixels to avoid artifacts from the circular shift of the ptychography reconstruction.

4. X-RAY OPTICS FABRICATION

The thin film stack was prepared by magnetron sputtering (Leica EM ACE 600, Germany) of a 100 nm thick Au film on a 100 nm thick SiN membrane with a window size of 500×500 μm on a 200-μm thick Si frame (Silson ltd, UK). The ion beam lithography was done using a dualbeam focused ion beam instrument (Nova Nanolab 600, FEI, Netherlands) with a pattern generator attachment (ELPHY MultiBeam, Raith GmbH, Germany). The design bitmap pattern was converted to a dot map GDSII stream file and used as input. The binarization, using a 0.15:0.85 line-to-space ratio, resulted in a pattern that can be machined using a process that resembles a single-pixel-single-pass process discussed in [3], and which resulted in the best pattern quality. The 60-μm wide computer-generated-hologram with 40-nm outermost width was milled using a 30-kV Ga+ ion beam and 50-pA current (19 nm nominal beam size) and 0.5-ms dwell time resulting in a dosage of 0.025 pC per dot.

5. CALCULATION OF RESOLUTION LIMIT

The theoretical limit on resolution is found by comparing the number of intensity measurements contained in the diffraction pattern M to the number of complex parameters in the object N. It is generally believed that, in order for the phase retrieval to be well posed, the number of intensity measurements must typically be greater than four times the number of complex parameters in the object [4, 5]. This belief is conditioned on relatively weak assumptions regarding the diversity of information contained within the individual measurements. We note that M is proportional to the area of the support of $\tilde{P} * \tilde{O}$ (the diffraction patttern). In contrast, N scales with the support of $\tilde{O}$, with the same constant of proportionality. In our test geometry, we use a circular zone plate which fills a ring in reciprocal space $\frac{k_p}{2} < |k| < k_p$ with random phase noise. The band-limiting constraint applied to the object, however, is a square such that $|k_x| < k_o$,$|k_y| < k_o$.

For $k_o > \frac{k_p}{2}$, the support of $\tilde{P} * \tilde{O}$ will be a rounded square covering an area of $A_I = \pi k_p^2 + 8k_p k_o + 4k_o^2$. The support of $\tilde{O}$ will simply be $A_O = 4k_o^2$. We can solve for the ratio, $R = \frac{k_o}{k_p}$, such that $A_I = 4A_O$, finding $R \approx 0.944$. In our paper, we chose to band-limit the object to a square region to allow for a simple computational approach and a well-defined interpretation of the resulting images. In a potentially more elegant reconstruction approach where the object is band-limited to a circular region in Fourier space, one finds the simpler result that the reconstructions are theoretically limited to $R = 1$.

This result should be considered as a limit on the potential reconstruction resolution of RPI rather than an estimate of the likely achievable resolution. In order for the reconstruction problem to be well posed at $M = 4N$, the measurement vectors must meet conditions which we do not guarantee. In addition, practical phase retrieval algorithms typically require more stringent constraints on the ratio of measurements to complex parameters to lead to convergence with high probability.

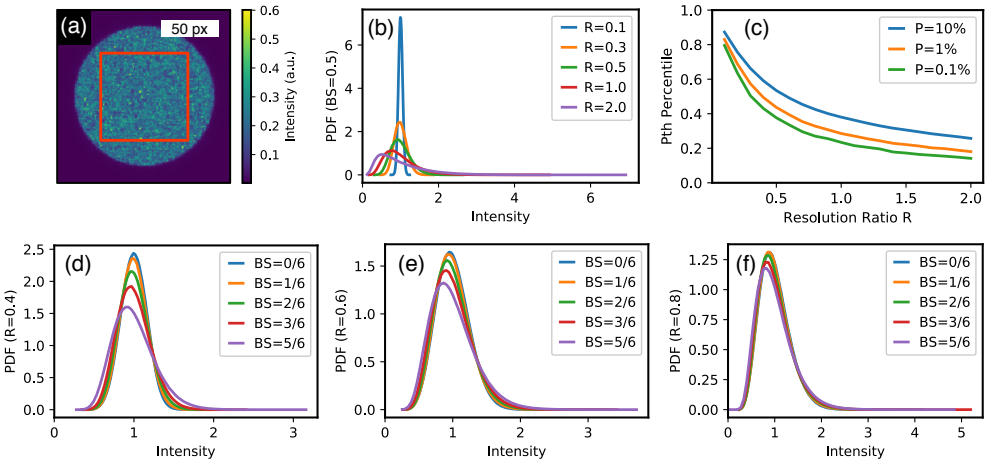

Fig. S3. Illumination Uniformity. (a), The distribution of intensities over the focal spot for $R = 0.6$, $BS = 0.5$, with the region used to extract the PDFs outlined in orange. (b) The intensity PDF arising from BLR light with $BS = 0.5$ at various resolution ratios. (c) The ratio of various percentiles to the median flux as a function of R for $BS = 0.5$. (d), (e), (f), The dependence of the illumination PDF on the beamstop diameter BS at $R = 0.4$,$R = 0.6$, and $R = 0.8$ respectively.

6. ILLUMINATION UNIFORMITY

One issue which arises when using structured illumination is a variation in the intensity of the light which interacts with each pixel of the low-resolution object. In a shot-noise limited experiment, this naturally leads to higher uncertainty in the reconstruction of weakly illuminated pixels. Other noise sources which uniformly affect the diffraction pattern are also expected to lead to higher errors in the reconstruction of weakly illuminated pixels.

Conceptually, one can break the intensity variations into two distinct categories. Most important are the high-frequency variations that manifest themselves in the network of zeros interpenetrating the illumination. However, in addition to these nodes between the speckles, the speckles themselves have nonuniform intensities. This variation becomes important at high R as the number of speckles per pixel decreases. Additionally, at large beamstop diameters correlations between neighboring speckles emerge. This reduces our ability to improve the uniformity by lowering R, because the various speckles within a low-resolution pixel remain correlated with one another.

To inspect the extent of this issue in RPI, we generated many BLR probes with $k_p = 128$ at a variety of beamstop diameters using the framework outlined in Supplementary Section 1. The beamstop diameters are defined by BS, the ratio of the beamstop diameter to the optic diameter. Then, we ran the forward model on low-resolution objects at a collection of resolution ratios R. For each pixel in the object, we recorded the total diffracted intensity resulting from an object with that pixel set to 1 and all others set to 0. This measures how sensitive the final diffraction pattern is to the complex free parameter associated with that pixel. We then studied the distribution of resulting intensities arising from the pixels within the illuminated field of view.

The results are presented in Figure S3. We find several important trends. The dominant trend is, as expected, an increase in the intensity variation with resolution ratio, R, at all beamstop diameters. In addition, illumination with a smaller diameter beamstop leads to smaller deviations at low R. This is a result of the beamstop-induced low-frequency intensity correlations. Nevertheless, we find that the distribution of intensities remains relatively small in the region $R < 0.6$ where reconstructions are experimentally feasible. This remains true even when using a beamstop with the extraordinarily large diameter of $\frac{5}{6}$.

In conclusion, the illumination non-uniformity is likely to become an increasingly relevant issue if algorithmic improvements allow for numerically stable reconstructions at values of R closer to 1. However, for currently feasible reconstruction ratios and standard beamstop diameters, the variability in illumination is tolerable. To be specific, at $R = 0.6$ and $BS = 0.5$, 99.9% of all pixels

are illuminated by light which is at least 0.39 times as intense as the flux through the median pixel.

7. APPLICATION RECOMMENDATIONS

First, we discuss recommendations for ptychography beamlines interested in adding a new zone plate to enable RPI. The most important parameter to consider is the numerical aperture of the randomized zone plate. In cases where the numerical aperture of the detector is large enough to enable reconstructions below a full pitch resolution of 20 nm, the appropriate zone plate numerical aperture is likely to be "as high as possible", because it may not be practical to design a zone plate with a numerical aperture large enough to fill the detector.

However, in a situation where it is possible to design such a zone plate with a numerical aperture matched to a detector, we recommend choosing a zone plate design which fills roughly $\frac{2}{3}$ of the detector at the lowest commonly used energy. This is because RPI reconstructions are likely to be reliable out to a resolution ratio of $R \approx 0.5$. For a zone plate which fills $\frac{2}{3}$ of a detector, the highest reconstructed object frequencies at $R = 0.5$ will be pushed exactly to the edge of the detector. One is tempted to increase the filling of the detector, however there is an advantage to leaving a portion of the detector unfilled. Because the high frequency components of an object are typically much weaker than the low-frequency ones, overfilling a detector with a high NA zone plate will swamp all the high frequency components with Poisson noise from the intense low frequency region. The portion of the diffraction pattern beyond the zone plate filling only includes high frequency components, and it is therefore desirable to capture it on the detector.

In all cases, we recommend designing the zone plate such that its focal spot fills roughly 80% of the detector conjugate coordinate space at the highest commonly used energy. It may seem ideal to simply fill this space to get the most out of each pixel. An obvious downside is that, as the real space oversampling decreases, the finite pixel size on the detector leads to a reduced speckle contrast. In addition, including a small region around the focal spot allows some room for the probe to be defocused and therefore reduces the complexity of probe alignment. We finally note that, if a large energy range is used at a beamline, it may be worthwhile to design a collection of zone plates optimized for use at different energies.

We next discuss the issues that are relevant when designing a system from the ground up with RPI in mind. First, and most obviously, one must have set of motors capable of reliably scanning a test sample through the beam with accuracy high enough for ptychography to succeed. Second, there is an incentive to use a detector with as many pixels as possible. This is, unsurprisingly, because the space bandwidth product of the final RPI reconstruction will be related to the number of pixels in the detector. Fortunately, randomized zone plates lead to ptychography and RPI reconstructions which are robust to missing data, so there are no major issues with using segmented detectors to increase the pixel count.

If one is interested in the highest resolution imaging, it is prudent to design the highest numerical aperture zone plate which is reasonable, and ensure that the detector can subtend a numerical aperture which is at least $\frac{3}{2}$ times that. If one is interested in capturing lower resolution images with a larger field of view, it may be more appropriate to start by designing a detector geometry which leads to the desired field of view before designing a zone plate to match that detector's numerical aperture. Finally, designing with beamline stability in mind is especially critical, because a well characterized beamline would (for example) enable energy or polarization sweeps without the need for repeat calibration ptychography scans.

REFERENCES

1. S. Marchesini and A. Sakdinawat, "Shaping coherent x-rays with binary optics," Opt. Express **27**, 907–917 (2019).
2. M. Van Heel and M. Schatz, "Fourier shell correlation threshold criteria," J. Struct. Biol. **151**, 250–262 (2005).
3. K. Keskinbora, U. T. Sanli, M. Baluktsian, C. Grévent, M. Weigand, and G. Schütz, "High-throughput synthesis of modified Fresnel zone plate arrays via ion beam lithography," Beilstein J. Nanotechnol. **9**, 2049–2056 (2018).
4. R. Balan, P. Casazza, and D. Edidin, "On signal reconstruction without phase," Appl. Comput. Harmon. Analysis **20**, 345–356 (2006).
5. A. S. Bandeira, J. Cahill, D. G. Mixon, and A. A. Nelson, "Saving phase: Injectivity and stability for phase retrieval," Appl. Comput. Harmon. Analysis **37**, 106–125 (2014).